A Structure-Based Approach to Ligand Discovery for 2*C*-Methyl-D-erythritol-2,4-cyclodiphosphate Synthase: A Target for Antimicrobial Therapy†

Nicola L. Ramsden,‡ Lori Buetow,‡ Alice Dawson,‡ Lauris A. Kemp,‡ Venkatsubramanian Ulaganathan,‡ Ruth Brenk,‡,§ Gerhard Klebe,§ and William N. Hunter*,‡

Division of Biological Chemistry and Drug Discovery, College of Life Sciences, University of Dundee, Dow Street, Dundee, DD1 5EH, Scotland, United Kingdom, Institut für Pharmazeutische Chemie, Philipps-Universität, Marburg, Marbacher Weg 6, 35032 Marburg, Germany

Received November 24, 2008

The nonmevalonate route to isoprenoid biosynthesis is essential in Gram-negative bacteria and apicomplexan parasites. The enzymes of this pathway are absent from mammals, contributing to their appeal as chemotherapeutic targets. One enzyme, 2*C*-methyl-D-erythritol-2,4-cyclodiphosphate synthase (IspF), has been validated as a target by genetic approaches in bacteria. Virtual screening against *Escherichia coli* IspF (*Ec*IspF) was performed by combining a hierarchical filtering methodology with molecular docking. Docked compounds were inspected and 10 selected for experimental validation. A surface plasmon resonance assay was developed and two weak ligands identified. Crystal structures of *Ec*IspF complexes were determined to support rational ligand development. Cytosine analogues and Zn^{2+}-binding moieties were characterized. One of the putative Zn^{2+}-binding compounds gave the lowest measured K_D to date (1.92 ± 0.18 μM). These data provide a framework for the development of IspF inhibitors to generate lead compounds of therapeutic potential against microbial pathogens.

Introduction

All isoprenoids are derived from two precursors, dimethylallyl diphosphate and isopentenyl diphosphate. The biosynthesis of these simple five-carbon compounds, which contribute to a plethora of important metabolites and natural products, is an important area of chemical biology. The precursors are either synthesized via the classical mevalonate pathway (MVA[a])[1] or the more recently discovered nonmevalonate pathway.[2−4] The MVA pathway is present in animals, fungi, the cytoplasm of phototrophic organisms, some eubacteria, and archaea,[4−6] whereas the nonmevalonate pathway is present in most eubacteria,[4] in the chloroplasts of phototrophic organisms such as algae, liverworts, and higher plants,[6] and in cyanobacteria and diatoms.[7] It is also found in unicellular eukaryotes with an evolutionary linkage to photosynthetic phyla, such as *Prototheca wickerhamii*[8] and *Plasmodium sp.*[4,9] On the basis of chemical and genetic data, the enzymes of the nonmevalonate pathway are deemed attractive chemotherapeutic targets.[4] They are absent from humans and occur in many of the world's most serious pathogenic microorganisms, including *Mycobacterium tuberculosis* and *Plasmodium falciparum*, the causal agents for tuberculosis and malaria, respectively.[9−12] There are seven enzymes in the pathway, and gene knockouts indicate that all are essential in bacteria.[4,10,12,13] Such genetic validation is complemented by the chemical validation of 1-deoxyxylulose 5-phosphate (DOXP) reductoisomerase (IspC), the second enzyme in the pathway, using the antimicrobial fosmidomycin.[11,14] The subject of this study is the fifth enzyme in the pathway, 2*C*-methyl-D-erythritol-2,4-cyclodiphosphate (MECDP) synthase, or IspF. This enzyme converts 4-diphosphocytidyl-2*C*-methyl-D-erythritol-2-phosphate into MECDP and CMP (Figure 1).[15] Structural and biochemical studies of IspF from several species have been reported.[16−25] IspF forms a homotrimer built around a β prism with three active sites, each of which is formed in a cleft between pairs of subunits.[16−18] The active site comprises a rigid, nucleotide-Zn^{2+}-binding pocket and a flexible loop to bind the 2*C*-methyl-D-erythritol-2-phosphate (ME2P) fragment of the substrate. A second divalent cation (Mg^{2+} or Mn^{2+}), positioned between the α- and β-phosphates of the substrate, acts in concert with the Zn^{2+} to align and polarize the substrate for catalysis.[16,18] We have adopted a structure-

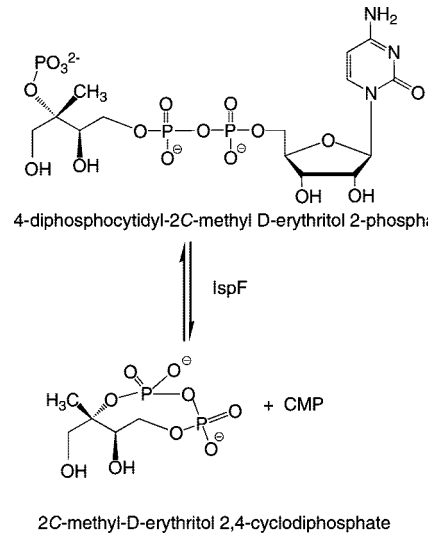

Figure 1. The reaction catalyzed by IspF.

† The coordinates and structure factors have been deposited in the Protein Data Bank with accession codes 3ELC (FLUC), 3EOR (CVD), 3ERN (AraCMP), 3ESJ (**7**), and 3FBA (**6b**).

* To whom correspondence should be addressed. Phone: +44 1382 345745. Fax: +44 1382 345764. E-mail: w.n.hunter@dundee.ac.uk

‡ Division of Biological Chemistry and Drug Discovery, College of Life Sciences, University of Dundee.

§ Institut für Pharmazeutische Chemie, Philipps-Universität, Marburg.

[a] Abbreviations: AraCMP, cytosine arabinoside monophosphate; CDV, cidofovir; DMSO, dimethylsulfoxide; DOXP, 1-deoxyxylulose 5-phosphate; *Ec*, *Escherichia coli*; FLUC, 5-fluorocytidine; IspC, 1-deoxyxylulose 5-phosphate reductoisomerase; IspF, 2*C*-methyl-D-erythritol-2,4-cyclodiphosphate synthase; ME2P, 2*C*-methyl-D-erythritol-2-phosphate; MECDP, 2*C*-methyl-D-erythritol-2,4-cyclodiphosphate; *Mt*, *Mycobacterium tuberculosis*; MVA, mevalonate; PDB, Protein Data Bank; *Pf*, *Plasmodium falciparum*; SPR, surface plasmon resonance.

10.1021/jm801475n CCC: $40.75
Published on Web 03/25/2009

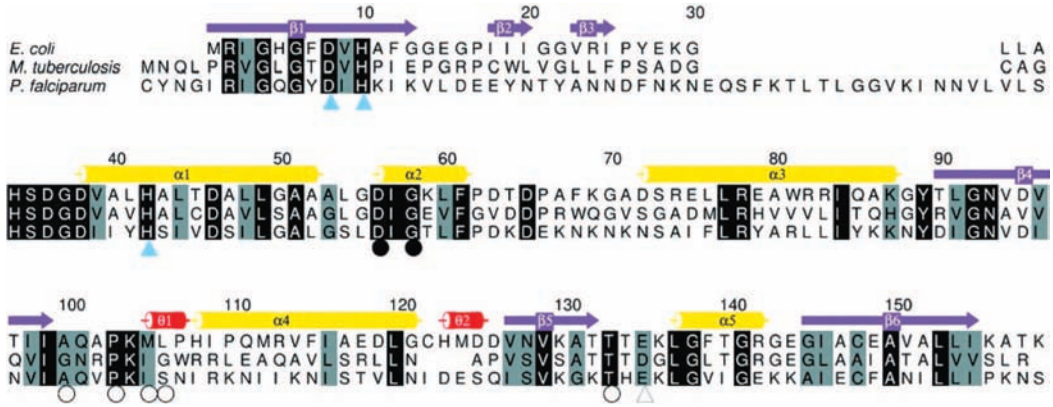

Figure 2. Sequence alignment of IspF from *E. coli*, *M. tuberculosis*, and the catalytic domain of the *P. falciparum* protein. The secondary structure of *Ec*Ispf is depicted as purple arrows for β-strands, yellow cylinders for α-helices, red cylinders for 3_{10}-helices. Residues whose identity is strictly conserved in all three sequences are boxed in black, conservative substitutions in gray. Grey triangles mark three residues that coordinate Zn^{2+}, and an open triangle the Mg^{2+}/Mn^{2+}-binding Glu-135. Circles mark CDP-binding residues (open and filled to distinguish subunits). The highly conserved segment leading into a1 forms the ME2P binding site.

based approach to identify inhibitors of IspF and screened, *in silico*, a database of commercially available compounds against the nucleotide-Zn^{2+}-binding pocket. The structure of *E. coli* IspF (*Ec*IspF) bound to CDP[16] was used to identify features considered important for ligand binding and affinity. A hierarchical filtering methodology and molecular docking with FlexX[26] generated several hits, which were then verified with X-ray crystallography and a surface plasmon resonance (SPR) assay. In addition, a more focused set of compounds was used to probe the cytidine and Zn^{2+}-binding sites, yielding a ligand with low micromolar binding affinity.

Results and Discussion

Protein Structure Selection. The selection of the protein structure to provide the template for ligand discovery is critical because the performance of molecular docking depends on the conformation of the active site residues of the target. Although our ultimate interest is to discover inhibitors of *P. falciparum* (*Pf*IspF) and *M. tuberculosis* (*Mt*IspF), these structures are not known, and *Ec*IspF was selected as the template for virtual screening based on a number of criteria. The *Ec*IspF enzyme is the best characterized following detailed biochemical analyses and with high resolution crystal structures available of the enzyme bound to a number of ligands including the substrate and product. There is high overall sequence homology between the active sites of *Ec*IspF, *Pf*IspF, and *Mt*IspF. The residues that coordinate the two divalent cations are conserved, as are the residues that interact directly with the substrate (Figure 2).[16,21] In addition, the established protocols for overexpression, purification, and crystallization of *Ec*IspF facilitated experimental validation of putative ligands.

We decided to concentrate efforts on the cytidine-binding pocket. This section offers a relatively static part of the active site in comparison to the ME2P-binding pocket. Twelve crystal structures of *Ec*IspF were available, and selection criteria were applied to select one for virtual screening. Structures that did not contain a ligand were eliminated and because the Zn^{2+}-binding site comprised part of the target, structures without this cation were also discarded. The remaining choices were complex structures of *Ec*IspF bound to CMP, CDP, or product (CMP and MECDP). *Ec*IspF−CMP complexes were eliminated because CMP is a substructure of the CDP and product complexes. In some instances, redundant complexes were present and the highest resolution structure was selected. At the end of this process, two structures of *Ec*IspF remained: *Ec*IspF-CDP (Protein Data Bank (PDB) code 1GX1, at 1.8 Å resolution) and *Ec*IspF−CMP−MECDP (PDB 1H48, 2.3 Å resolution). The *Ec*IspF−CDP structure was chosen by virtue of the higher resolution of the analysis.

Validation of FlexX with EcIspF for Virtual Screening. It was first necessary to assess the suitability of FlexX[26] for our modeling, and it was used to generate binding modes of CDP in the active site of *Ec*IspF. FlexX can apply two scoring functions, F-Score and DrugScore, to rank binding modes, and both were evaluated. In addition, the quality of each binding pose was assessed by the root mean squared deviation (rmsd) of atomic positions between the calculated and experimentally determined binding modes. The ligand poses that are generated are defined as "well-docked" if they display an rmsd of less than 2.0 Å from the experimental structure.[27] When CDP was docked back into the active site of 1GX1, only 70% of the top 20 poses ranked by F-Score had rmsd values significantly less than this threshold value compared to 100% by DrugScore. The closest generated pose, which was ranked ninth by DrugScore, was within 0.6 Å of the experimental conformation (data not shown). These results demonstrate the suitability of FlexX/DrugScore and the applied docking protocol for this enzyme.

Hierarchical Filtering and Virtual Screening. We adopted a three-step hierarchical filtering approach, removing compounds based on molecular complexity, topology, and functionality.[28,29] Initially, filters were applied to a database of approximately 1 million commercially available compounds so that only those with less than seven rotatable bonds and a molecular mass below 450 Da were retained. These criteria are based on theoretical[30] and empirical[31] arguments, suggesting that lead compounds should be of limited complexity to allow for subsequent lead optimization. In the second step, a three-dimensional pharmacophore hypothesis was constructed based on the interactions formed between CDP and *Ec*IspF.[16] This pharmacophore hypothesis (Figure 3) was composed of a hydrophobic component (H), centered on the pyrimidine of CDP, a hydrogen bond donor group (D1) based on the exocyclic amine group, and two hydrogen bond acceptor groups derived from N3 (A2) and O2 (A3) of cytosine (Figure 3). The hydrogen bond partners on *Ec*IspF that complement the pharmacophore are the hydroxyl group of Thr133 (A1) and the main chain amides of Met103 (D2) and Leu106 (D3), respectively (Figure 3). The pharmacophore filtering procedure selected 4063 compounds, which were docked into the *Ec*IspF active site. Spatial constraints of 1.0 Å for the hydrophobic feature and 0.7 Å for donor and

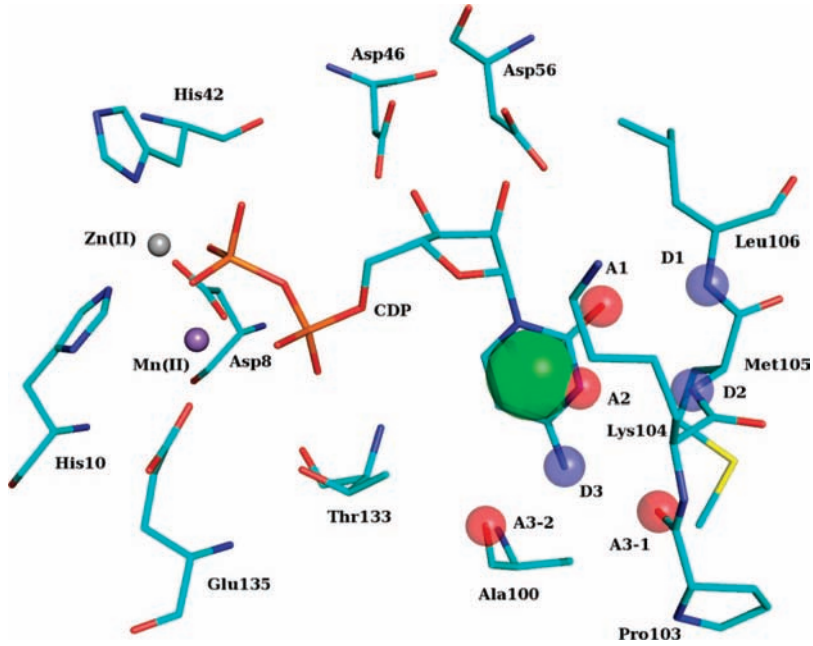

Figure 3. The pharmacophore hypothesis for inhibition of *Ec*IspF. CDP is shown as a stick model together with the two metal ions (Mn^{2+} purple sphere and Zn^{2+} gray sphere) and key residues in the active site of *Ec*IspF. Atoms are colored C cyan, N blue, O red, P orange, S yellow. The large red spheres mark hydrogen bond accepting groups of the ligand (A1 and A2) and the protein (A3-1 and A3-2), the blue spheres mark hydrogen bond donor sites on the protein (D1, D2) and the ligand (D3), and the green sphere identifies the hydrophobic component centered on the pyrimidine ring.

acceptor features were applied in order to match the same type of chemical interactions of potential ligands with those observed in the *Ec*IspF−CDP complex. The top 250 hits were inspected visually, and 10 compounds selected for experimental validation (Table 1) based on a number of criteria. It was judged important that there was a complementarity of the ligand and protein surfaces, reasonable internal geometry of the ligand in the binding pose, proximity of the hydrophobic center of the ligand to the cytosine binding pocket, and that reasonable hydrogen bonding interactions, typically with the separation of donor and acceptor groups in the range 2.4−3.5 Å, were predicted.

Binding Affinities of Compounds to EcIspF. An SPR assay with immobilized *Ec*IspF was developed (Figure 4) in order to determine the binding affinities of the selected compounds (Table 1). Five of these compounds required significant concentrations of dimethyl sulfoxide (DMSO) in order to dissolve, compromising the use of SPR. Consequently, binding for five of the compounds was analyzed. A series of concentrations of each compound ranging from 0.1 μM to 10 mM were applied for the assay. The binding responses were recorded as a function of time and, at all compound concentrations, the responses reached equilibrium and dissociated rapidly, indicating that binding was reversible. Only compounds **6** and **7** yielded quantifiable data. Values for K_D were obtained by fitting the steady-state binding curves to a 1:1 Langmuir binding model. Compounds **6** and **7** are weak ligands, having K_D values of 20.5 ± 2.23 and 0.925 ± 0.71 mM, respectively. The binding affinities of CMP (0.903 ± 0.107 mM) and CDP (0.097 ± 0.006 mM) were also determined, for the first time, for reference.

CDP binds *Ec*IspF at least 10-fold more tightly than CMP, **6**, or **7**. Compounds **6** and **7** are both CMP analogues and, like CMP, lack a β-phosphate. This suggests a significant contribution of the β-phosphate to ligand affinity, and we note in the structure of *Ec*IspF that this group coordinates the active site Zn^{2+}. Despite their structural similarity, the binding affinities of **6** and **7** vary. The K_D of **7** is comparable to that of CMP, but **6** binds about 20-fold weaker. Crystal structures of these ligands bound to *Ec*IspF were determined to investigate this observation.

Structural Characterization of Active Compounds. Co-crystallization of *Ec*IspF with compounds **6** and **7** gave crystals that diffracted to 3.1 and 2.7 Å resolution, respectively (Table 2). However, the observed electron and difference density maps suggested that hydrolysis has occurred at the ribose O2′ of **6**, producing a nonbridging phosphate at the 3′ position; therefore **6b** (Table 1) was modeled and refined satisfactorily. For discussion purposes, the experimental ligand and protein active site conformations are compared to CDP bound to *Ec*IspF (PDB 1GX1) because this provided the template for docking. As predicted, the compounds bind within the cytidine-binding pocket of *Ec*IspF. There are no major conformational changes in the enzyme upon ligand binding as evidenced by the rmsd differences (0.33, 0.29 Å) between Cα atoms of the compound−enzyme complexes **6b** and **7** with 1GX1. The largest Cα rmsd differences occur in the flexible loop (residues 62−71) that binds ME2P. This loop is poorly ordered in the absence of a ligand.[16,18]

Compound **7** comprises a cytosine, ribose, and phosphate similar to CMP, but the phosphate bridges ring positions 3 and 4 (Table 1). Despite this difference, a structural comparison demonstrates that **7** resembles the CMP fragment of CDP in its mode of binding (Figure 5); all protein ligand interactions are maintained except for those involving the β-phosphate of CDP, which has no counterpart in **7**. The cytosine moieties of both ligands bind, forming a network of interactions to main chain atoms of Ala100, Met104, Met105, and Leu106.[16] We note the possibility that a bifurcated hydrogen bond is formed between the amide of Met103 and the pyrimidine N3 and O2 (Figure 5a). The ligand O2′ hydroxyl forms hydrogen bonds to the carboxylate of Asp56 from one subunit and water-mediated hydrogen bonds to the amide of Ala131 of a second subunit. Compound **7** interactions with *Ec*IspF vary from those of CDP in that the phosphate binds the side chain hydroxyl of Thr133 through a water-mediated interaction rather

Table 1. Potential IspF Ligands Identified by Virtual Screening[a]

Number	Structure	K_D (mM) 10°C, pH 7
1	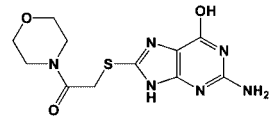	n.d
2	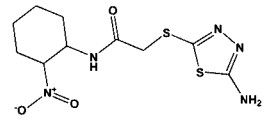	n.d
3	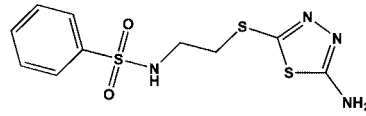	n.d
4	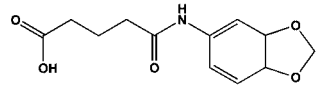	Inactive
5	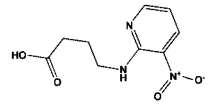	n.d
6	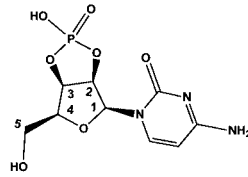	20.5 ± 2.2
6b	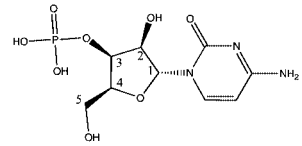	n.d.
7	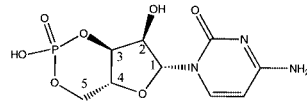	0.9 ± 0.7
8	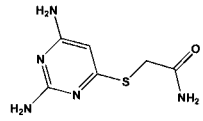	Inactive
9	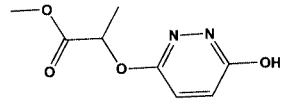	n.d
10	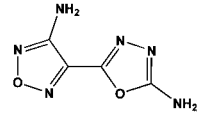	Inactive

[a] Compound **6b** was not identified by virtual screening but is a derivative of **6** likely generated following hydrolysis and was identified following the crystal structure determination (see text). The ribose rings are numbered for **6**, **6b**, and **7**. n.d. = not determined.

than a direct interaction, and there is an additional water-mediated hydrogen bond linkage to the main chain carbonyl of Phe61. The comparable binding affinities of **7** and CMP are clearly due to their chemical similarity and equivalent binding interactions with *Ec*IspF.

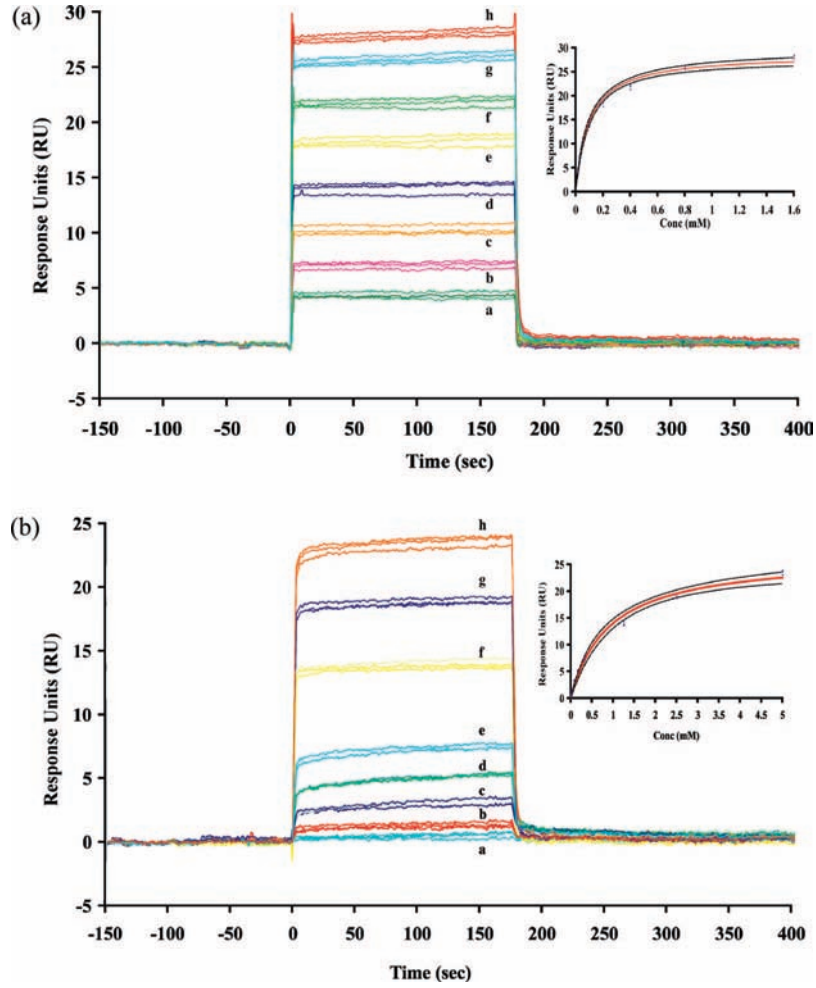

Figure 4. Representative binding sensorgrams of CDP (a) and CMP (b) to covalently immobilized *Ec*IspF. Reference-corrected SPR binding curves for various concentrations of CDP and CMP monitored on a surface with ~5000 RU of amine coupled *Ec*IspF. The data were globally fitted using a kinetic model where a 1:1 complex is formed between *Ec*IspF and CDP or CMP. The small graphs show the steady state (equilibrium) RU after fitting vs the concentrations of CDP or CMP. Running buffer was 50 mM sodium phosphate (pH 7), 2 mM $MgCl_2$ and 0.005% surfactant P20. In graph (a), curve a = 25 μM CDP; b = 50 μM CDP; c = 100 μM CDP; d = 200 μM CDP; e = 400 μM CDP; f = 800 μM CDP; g = 1.6 mM CDP. In graph (b), curve a = 78.1 μM CMP; b = 156.2 μM CMP; c = 312.5 μM CMP; d = 625 μM CMP; e = 1.25 mM CMP; f = 2.5 mM CMP; g = 5 mM CMP. Insets in (a) and (b): Nonlinear steady-state affinity analysis for the corresponding interaction. The curve drawn is the best-fit curve to a single-site binding equation with the program GraphPad Prism. This provides an apparent K_d of 96.59 ± 6.45 μM for CDP and 903.63 ± 10.77 μM for CMP.

Compound **6** was selected to probe the specificity of the binding pocket for different sugars as well as phosphate placement. This compound contains a cytosine and a lyxose with a phosphate bridging the 2 and 3 ribose positions (Table 1). Compound **6** was supplied as a mixture of anomers, but the experimental density suggested that only the β-anomer of the hydrolysis product **6b** has bound (Figure 5b). Steric clash between the α-anomer O5′ and side chains of Asp56 or Leu106 is the likely explanation for this observation. Despite this unexpected modification to the purchased compound, the network of interactions between the cytosine moiety of compound **6b** and *Ec*IspF is similar to that observed in the complex with CDP. The binding interactions between the **6b** sugar and *Ec*IspF resemble those observed between the ribose of CDP and the enzyme. The O2′ and O4′ groups of both sugars form hydrogen bonds with the side chains of Asp56 and Lys104, respectively. The orientation and interactions of the phosphates in C7 and **6b**, however, vary from those observed in CDP (Figure 5c,d). In the complex with **6b**, the phosphate is directed toward the Zn^{2+}-binding site rather than forming a hydrogen bond to the Thr132 side chain hydroxyl and an electrostatic interaction with Mn^{2+} as observed in the CDP complex.[16] The phosphate of **6b** forms solvent-mediated hydrogen bonds with the side chains of Asp46, Asp56, Thr132, and Thr133, the amide of Gly58, and the carbonyl of Ala131. The effects on binding affinity of replacing ribose with lyxose and changing the phosphorylation site are indeterminable because the relative quantities of the anomers and the amount of hydrolyzed ligand, present under assay conditions, are unknown.

Comparison of Predicted vs Experimental Binding Modes. Comparison of models obtained by the computational docking approach with structures determined by X-ray crystallography give an indication of how reliable predictive modeling can be for a specific system and may suggest where receptor/target flexibility or inflexibility can affect ligand binding. The predicted and experimental poses of **7** have an rmsd difference of 0.92 Å. The predicted interactions between the protein and the cytosine moiety of the top ranked binding conformation of **7** are similar to those observed in the *Ec*IspF−CDP complex (Figure 5e), but the binding interactions of the ligand sugar and phosphate with the protein differ due to side chain movements, changes in the flexible ME2P-binding loop, and slight differences in ligand conformation and placement (data not shown). In the docked complex, a phosphate oxygen and O5′ are 2.9

Table 2. Data Processing and Refinement Statistics of *Ec*IspF Ligand Complexes

ligand code	**6b**	**7**	AraCMP	FLUC	CDV
Crystal morphology	cube	cube	plate	plate	cube
X-ray source	ID29	ID29	ID29	RU-200	RU-200
wavelength (Å)	0.9756	0.9756	0.9756	1.5418	1.5418
space group	$I2_13$	$I2_13$	$P2_1$	$C2$	$I2_13$
unit cell:					
a (Å)	144	144.5	88.8	104.68	145.68
b (Å)			54.2	54.83	
c (Å)			118.4	88.51	
β (deg)			95	99.66	
resolution range (Å)	29.4−3.1	29.5−2.7	20−2.1	50−2.5	29.7−2.8
no. of measurements[a]	111733	202013	329171	382131	186443
no. of unique reflections	9178	13944	71490	15989	12818
redundancy	12.5	14.5	4.6	27.04	14.5
overall completeness (outer shell, %)[b]	99.9 (96.6)	99.9 (97.8)	94.3 (71.8)	91.4 (80.4)	99.9 (97.6)
mean $\langle I/\sigma(I)\rangle$	23.6 (7.3)	24.2 (8.9)	18.4 (1.6)	8.1 (2.2)	30.4 (5.0)
R_{sym} (%)[b]	10 (32.6)	9.9 (27.4)	8.9 (47.7)	8.5 (20.3)	8.7 (47.6)
solvent content (%)	80	80	50	45	80
monomers per a.u.[c]	1	1	6	3	1
R_{free}/R_{work} (%)	21.9/18.7	21.8/18.4	23.7/21.8	29.1/20.8	19.9/16.0
protein residues	157	162	942	471	157
water molecules	37	97	284	113	42
average B values (Å^2)					
protein	60.7	33.5	33.3	49.6	55.5
main chain	60.3	33.0	32.0	49.3	54.6
side chain	61.2	34.0	34.8	49.9	56.4
solvent	54.8	34.4	38.0	45.1	59.9
ligand	58.4	42.2	45.7	58.5	62.6
bond length rmsd (Å)	0.012	0.013	0.009	0.012	0.023
bond angle rmsd (deg)	2.22	1.55	1.24	1.41	2.02

[a] As reported in SCALA, including partials. [b] Values in parentheses refer to the highest resolution shell of about 0.1 Å width. [c] a.u. = asymmetric unit.

and 2.5 Å from CD1 of Ile57 and the side chain of Asp63. In the crystal structure, χ_1 of Ile57 has changed so that CD1 is shifted away from the ligand phosphate, the Asp63 side chain has adjusted position, and the ligand is displaced from the predicted binding site by approximately 0.6 Å to alleviate these close contacts (data not shown). The crystal structure also identifies a shift in the side chain of Lys104 to form a hydrogen bond to O4′ of the ligand (Figure 5b), an interaction not predicted in the modeled complex.

We did not dock compound **6b** in the active site of *Ec*IspF. In this case, the ligand has resulted from hydrolysis of compound **6**, which had been docked previously. Comparisons indicated that the position of the cytosine moieties agreed to the same extent as seen for comparisons with **7** (data not shown).

Analysis of Cytosine Analogues. Our aim is to obtain ligand scaffolds and through appropriate structural modifications to improve binding affinities. However, with limited structural diversity of potential *Ec*IspF ligands identified through virtual screening, in essence a single chemotype, it was decided to rationally select compounds to investigate the binding properties of part of the active site. Fluorescent substrate analogues have been used to examine the flexible loop that binds the substrate fragment ME2P and how this loop adjusts to a variety of aromatic scaffolds.[32] Here, we restricted our investigation to probing the cytidine- and Zn^{2+}-binding sites using cytosine analogues and common metal ion binding moieties, respectively. Both sets of compounds represent potential building blocks with beneficial pharmacokinetic properties and scope for optimization.

Three compounds were selected to investigate how small modifications to the ribose and cytosine moieties affect binding. Cidofovir (CDV), cytosine arabinoside monophosphate (AraCMP), and 5-fluorocytidine (FLUC) were chosen to probe the effects, respectively, of removing the sugar, altering chirality at C2′, and of whether a particular covalent modification on the cytosine ring was tolerated (Table 3). AraCMP and CDV are drugs used in cancer and viral therapies.[33,34] The complex structures of AraCMP, FLUC, and CDV with *Ec*IspF were determined to 2.1, 2.5, and 2.8 Å resolution (Table 2), respectively, and ligand binding affinities determined using SPR (Table 3). Most of the protein residues are well defined in the electron density maps for all structures except for residues 62−71, which form the flexible ME2P binding site and are poorly ordered. There are no major conformational changes upon ligand binding, as evidenced by the rmsd differences of 0.27, 0.36, and 0.25 Å for the overlay of Cα atoms of the compound−enzyme complexes FLUC, AraCMP, and CDV, respectively, with the CDP complex, PDB code 1GX1. The crystal structures of the complexes confirm that the ligands are firmly anchored in the cytidine-binding pocket (Figure 6). The cytosine moiety of each ligand forms the same network of interactions to the main chain of Ala100, Lys104, Met105, and Leu106, as observed in the complex with CDP.[16] AraCMP, FLUC, and CDV bind in a similar manner to CMP and CDP (Figure 6).

The asymmetric unit of the *Ec*IspF−AraCMP complex crystal structure contains six subunits. Five of the active sites are occupied by ordered AraCMP molecules, and the protein−ligand interactions (Figure 6a) are identical in each case. To prevent steric clash of the O2′ hydroxyl with Asp56 and Ala131, the cytosine moiety of AraCMP moves slightly away from the backbone of *Ec*IspF compared to the CMP fragment of CDP (data not shown). This allows the formation of a hydrogen bond between O2′ and the carbonyl of Ala131. O2′ also participates in a water-mediated interaction to the amide of Ala131. The O3′ group forms a water-mediated hydrogen bond with the amide of Gly58. This is in contrast to the interactions made by the O2′ and O3′ groups of CDP, which both form direct hydrogen bonds to the side chain of Asp56 and, for the latter only, to the amide of Gly58.[16] Like the CMP fragment of CDP, the phosphate group of AraCMP interacts with side chain and main chain atoms of Thr132 and Thr133. Overall, AraCMP forms between 8 and 9 direct hydrogen bonds compared to

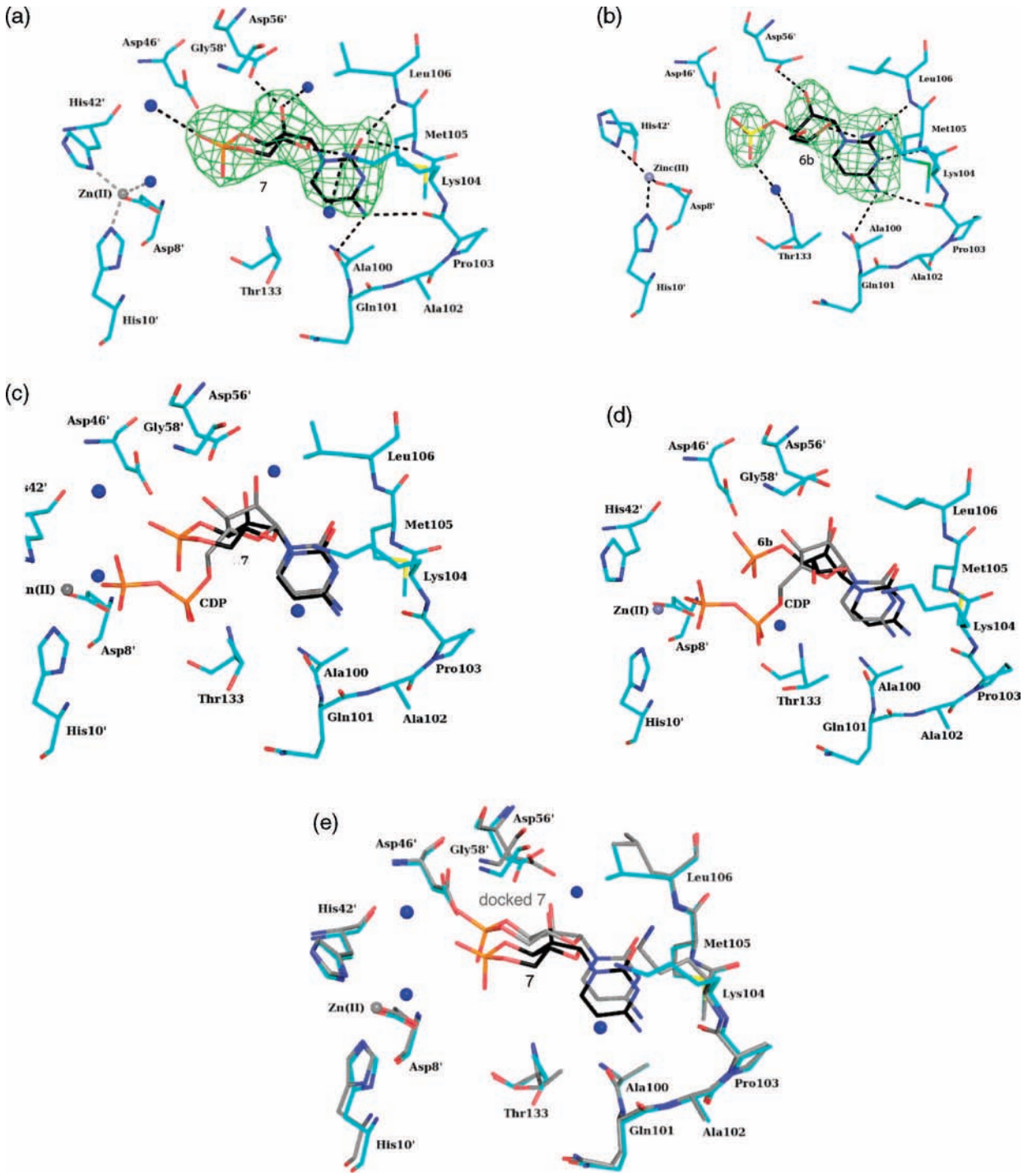

Figure 5. *Ec*IspF−ligand complexes. The active site of *Ec*IspF in complex with (a) **7**, (b) **6b**, (c) superposition of CDP on **7**, (d) superposition of CDP on **6b**, and (e) superposition of the top docked **7** pose in *Ec*IspF−CDP and *Ec*IspF−**7**. In (a) and (b), the $F_o - F_c$ omit map contoured at 3σ and colored green is shown and black dashed lines indicate putative hydrogen bonds. Zn^{2+} and water molecules are represented as gray and blue spheres, respectively, and the gray dashed lines represent metal ion ligand coordination. Protein residues labeled with a prime indicate that they belong to a partner subunit. Atoms are colored as followed: C atoms of the protein are cyan, N blue, O red, S yellow, P orange, ligand C atoms are black, and CDP and docked **7** C atoms are gray. In (e), C atoms of the protein in the *Ec*IspF−CDP complex are gray.

10−11 formed by CMP. AraCMP has a binding affinity of 18.9 ± 5.8 mM, which is 20-fold weaker than CMP (0.903 ± 0.107 mM). Although the active site can accommodate a change in chirality at C2′, this is accompanied by a large, unfavorable effect on binding affinity.

The same network of protein−pyrimidine interactions is observed in the FLUC complex (Figure 6b), although the cytosine pocket of the enzyme has expanded slightly to accommodate the additional substituent on the pyrimidine. The distance between the Cα atoms of Thr133 and Leu106 of the same subunit defines one dimension of the enzyme active site and is slightly longer in the FLUC complex (12.5 Å) compared to the CDP complex (11.9 Å). In the FLUC complex, the cytosine moiety shifts closer to Met105 and Leu106 compared to the CDP complex, allowing the formation of a hydrogen bond between the fluorine and main chain amide of Thr133. In the CDP complex, the α-phosphate accepts a hydrogen bond from this amide group. The pyrimidine shift in the FLUC complex

Table 3. Cytosine Derivatives[a]

	Common name	Structure IUPAC name	Mass (Da)	K_D (mM) 10°C, pH 7
AraCMP	cytosine arabinoside monophosphate	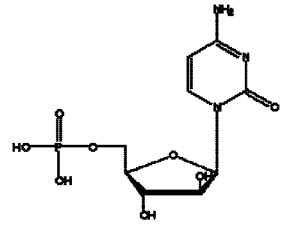 Phosphoric acid mono - [(2*R*,3*S*,4*S*,5*R*) - 5 - (4 - amino - 2 - oxo - 2*H* - pyrimidin - 1 - yl) - 3,4 - dihydroxy - tetrahydro - furan - 2 – ylmethyl] ester	243.2	18.91 ± 5.8
FLUC	5-fluorocytidine	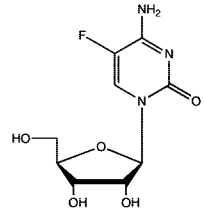 4-amino-1-[(2R,3R,4S,5R)-3,4-dihydroxy-5-(hydroxymethyl)oxolan-2-yl-5-fluoro-pyrimidin-2-one	261.2	2.02 ± 0.42
CDV	Cidofovir	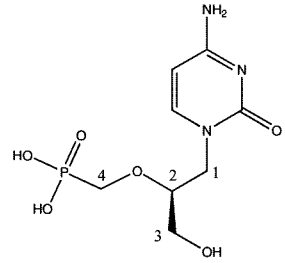 [(2R)-1-(4-amino-2-oxo-pyrimidin-1-yl)-3-hydroxy-propan-2-yl] oxymethylphosphonic acid	279.2	~40

[a] Ligand codes, names, structures, molecular weight, and binding affinities are given.

prevents O3′ from interacting with the side chain of Asp56 and causes the side chain of Leu106 to shift away from the ligand to prevent steric clash. Although FLUC has no phosphate group, the binding affinity (2.02 ± 0.42 mM) is similar to that of CMP (0.903 ± 0.107 mM), implying that the fluorine atom compensates for the loss of phosphate-derived electrostatic interactions. Binding of FLUC by *Ec*IspF suggests that additional pyrimidine substituents could be accommodated by the enzyme active site and further systematic investigation to determine the limits on the number, size, and chemical properties of additional substituents that can be accommodated are warranted.

The cytosine moiety of CDV forms the same interactions with the protein as previously described for CDP,[16] which are the only direct interactions with the protein; all other hydrogen bonds are solvent-mediated (Figure 6c). The interactions between the noncytosine fragment of CDV and protein resemble those solvent-mediated interactions formed between *Ec*IspF with the ribose and α-phosphate moieties of CDP. Solvent-mediated interactions between CDV and *Ec*IspF include ligand phosphate associations with the side chains of Asp56, Asp63, Thr132, and the amides of Ala131 and Thr133. The lack of direct hydrogen bonding interactions between the ligand and enzyme probably contributes to the weak binding affinity (~40 mM) of CDV for *Ec*IspF.

Analysis of Zn^{2+}-Binding Moieties. Hydroxamates and sulfonamides are among the most common Zn^{2+}-binding ligands.[35] Six compounds (Table 4), three hydroxamates (**11**−**13**), and three sulfonamides (**14**−**16**), were selected for this study based on commercial availability and mass to ensure that the putative ligands were small enough to bind within the *Ec*IspF active site. Cocrystallization of all six compounds with *Ec*Ispf was attempted, but, for reasons we cannot explain, no crystals were obtained. The sulfonamide compounds were only soluble in DMSO, thus hindering the SPR binding assay. The hydroxamates were soluble in assay buffer but no measurable data were obtained for **11** and **12**, probably due to their small mass. The change in refractive index for binding of a ligand smaller than 180 Da is likely too small to be detected on a BiaCore 3000 instrument (John Butler, personal communication). The SPR binding assay was able to quantify the binding affinity of **13**, yielding a K_D of 1.92 ± 0.18 μM. Compound

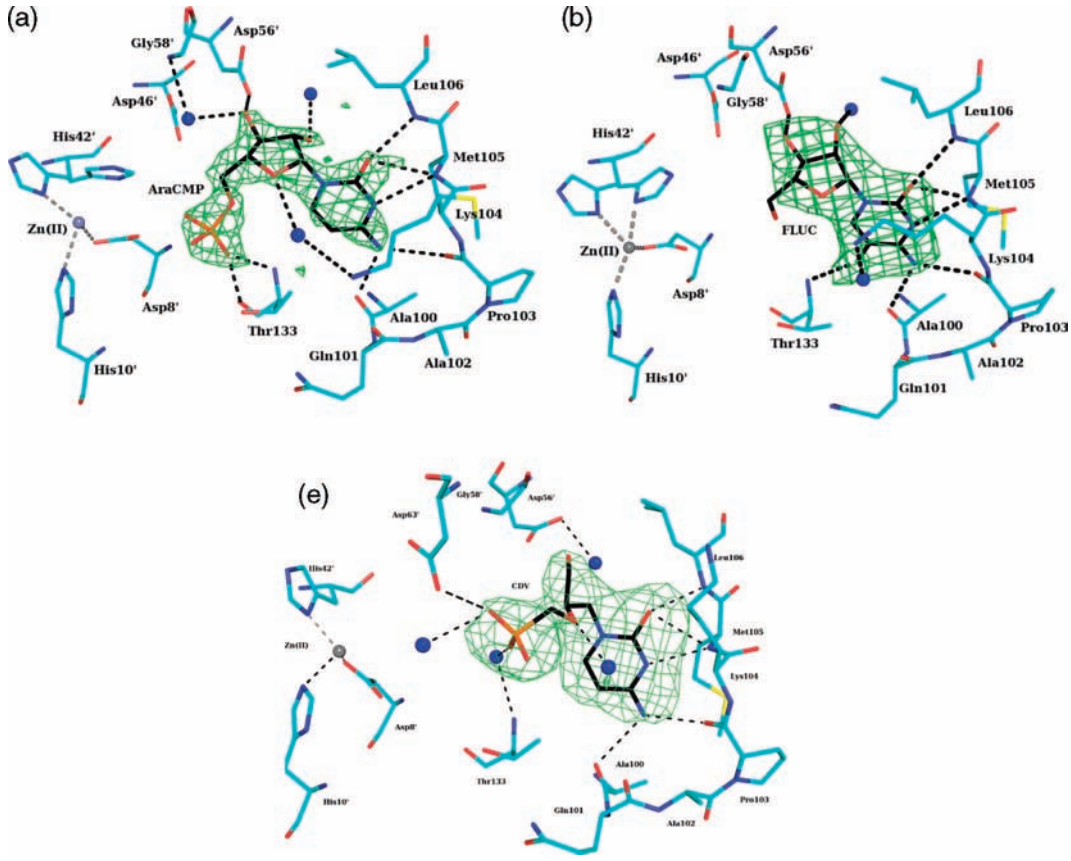

Figure 6. Cytosine-based compounds binding to *Ec*IspF. The active site of *Ec*IspF in complex with (a) AraCMP, (b) FLUC, and (c) CDV. In each case, the $F_o - F_c$ omit map is shown as green chicken wire and contoured at 3σ. The color scheme is similar to Figure 5.

13 has the highest affinity of all the ligands examined in this study, and we attribute this to Zn^{2+}-hydroxamate coordination. Similar observations apply to other Zn^{2+}-dependent enzymes, including *E. coli* LpxC, an enzyme in the lipid A biosynthesis pathway. Kinetic studies of LpxC revealed that replacing a carboxylate group on 4,5 dihydro-2-phenyloxazole-4-carboxylic acid with hydroxamate lowered the IC_{50} from >400 to 3 μM.[36] Our observations suggest that the addition of a Zn^{2+}-binding moiety may prove valuable in assisting the design of potent and selective inhibitors of *Ec*IspF. In this, one possible strategy could be to develop molecules tethered by a Zn^{2+}-binding moiety to the catalytic center, which then extend to the cytosine-binding pocket where very clear and conserved molecular features could assist the incorporation of specificity (Figure 1B). Because the Zn^{2+} location is within proximity of the ME2P binding site, then there is also the potential to extend from a metal-binding group using molecular fragments that mimic the methylerythritol component of substrate, a moiety that also interacts with a highly conserved part of the enzyme.

Ligand Efficiency to Compare Compounds. Previously reported fluorescent substrate analogues[32] have greater affinity for *Ec*IspF and a measurable gain in binding free enthalpy compared to the compounds in this study. Although potency is an important criterion for assessing lead compounds it can be misleading.[37] A useful parameter for assessing the potential of a weak lead for inhibitor design is to calculate the binding energy per non-hydrogen atom for each ligand, or 'ligand efficiency' (Δg).[38] This parameter was calculated using equation 1.1 for the compounds in this study (except **6**), and the substrate fragments CDP and CMP (Table 5).

$$\Delta g = \Delta G / N_{\text{non-hydrogen atoms}} \qquad (1.1)$$

where $\Delta G = -RT \ln K_d$ and N is the number of non-hydrogen atoms.

Interestingly, FLUC (-0.81 kJ·mol^{-1}/non-H atom) has a ligand efficiency comparable to CDP (-0.87 kJ·mol^{-1}/non-H atom) and CMP (-0.79 kJ·mol^{-1}/non-H atom). Although the fluorescent substrate analogues have greater potency, they have lower ligand efficiencies (-0.64 to -0.70 kJ·mol^{-1}/non-H atom) compared to CMP. The aromatic moieties added to the substrate-like entities benefit binding affinity,[32] but they do not improve ligand efficiency. Compound **13** has the best ligand efficiency with a Δg value of -2.04 kJ·mol^{-1}/non-H atom. This is significantly improved over CDP yet much weaker in comparison to the average value associated with a drug in clinical use (-6.3 kJ·mol^{-1}/non-H atom).[38]

Conclusions

In this study, virtual screening for potential ligands of *Ec*IspF was performed exploiting a hierarchical filtering methodology followed by molecular docking with the program FlexX. Application of an SPR assay and crystallographic studies has served to characterize two weak binding ligands. These initial results prompted further elucidation of the binding properties of *Ec*IspF by analyzing cytosine derivatives again using crystallography and SPR. The cytosine-binding site of *Ec*IspF can tolerate small structural modifications of the pyrimidine, as evidenced by binding of FLUC. Modifications to the ribose, particularly at C2′, are detrimental to binding affinity but do not preclude ligand binding as seen in the complexes with AraCMP and CDV. The incorporation of solvent mediated hydrogen-bonding interactions, linking functional groups on the ligands to the enzyme, appears to compensate for alterations in the structure of the ligands compared to substrate.

Generally, when a nucleoside or nucleotide represents a fragment of substrate, this fragment alone does not contribute

Table 4. Table of Selected Hydroxamate and Sulfonamide Compounds[a]

Number	Ligand Structure IUPAC name	Mass (Da)	K_d (μM) 10°C, pH 7
11	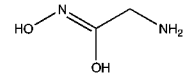 2-amino-*N*-hydroxy-acetimidic acid	90.1	n.d
12	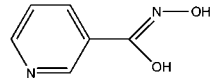 *N*-hydroxy-nicotinimidic acid	138.1	n.d
13	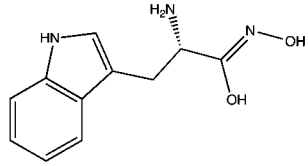 2-amino-*N*-hydroxy-3-(1*H*-indol-3-yl)-propionimidic acid	219.2	1.92 ±0.18
14	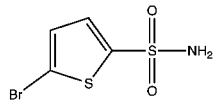 5-bromo-thiophene-2-sulfonic acid amide	242.1	n.d
15	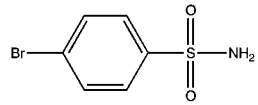 4-bromobenzenesulfonamide	236.1	n.d
16	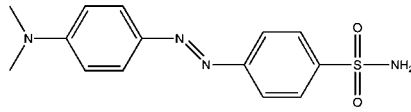 4-(4-dimethylamino-phenylazo)-benzenesulfonamide	304.4	n.d

[a] Ligand codes, names, structures, molecular weight (MW) and binding affinities are shown. n.d. = not determined.

significantly to binding affinity. This is clearly the case for the enzyme LpxC, which has a K_m >20 mM for UDP-GlcNAc and 2.1 μM for UDP-3-acyl-GlcNAc, the natural substrate.[39,40] In such cases, potent inhibition might best be sought by targeting part of the active site that does not belong to the nucleotide binding pocket. The tight binding of the hydroxamate **13**, postulated to bind the active site Zn^{2+}, provides support for incorporation of metal binding moieties to design potent inhibitors. While hydroxamates can lack specificity,[35] incorporation of such a group onto cytosine analogues offers potential as a strategy to improve selectivity and potency for novel inhibitors of *Ec*IspF.

Experimental Section

Hierarchical Filtering. We used the same virtual screening database that was compiled for a previous study.[29] In short, this database contained the three-dimensional structures of small molecules stored in the Available Chemicals Directory and of screening compounds supplied by five companies, namely Ambinter, Asinex, ChemStar, InterBioScreen, and Tripos. In total, 826952 commercially available compounds were stored in this database. Filtering for compounds that possessed at least two hydrogen bond donors, two hydrogen bond acceptors, and one hydrophobic region (a five- or six-membered ring) was performed using SELECTOR.[41] The pharmacophore search was performed using UNITY[42] with the Lipinski's "rule of five" check activated.[43]

Docking. Ligands were docked into the binding site of *Ec*IspF (PDB 1GX1) using FlexX v1.3.[26] The DrugScore[44] scoring function was applied during the placement and construction phase and for ranking.

Protein Preparation. All chemicals purchased were of the highest purity available. IspF was expressed in *E. coli* strain BL21 (DE3) and purified following published methods.[16] The protein concentration was determined spectrophotometrically using a theoretical extinction coefficient of 8370 $M^{-1}\cdot cm^{-1}$ at 280 nm and purity assessed as being

Table 5. Ligand Efficiency for Compounds Used in This Study

compd	mass (Da)	K_D (mM), 10 °C, pH 7	ΔG (kJ·mol^{-1})	no. of non-H atoms	ligand efficiency (Δg = kJ·mol^{-1}/non-H atom)
13	219.2	0.0019 ± 0.0002	−32.62	16	−2.04
CDP	403.2	0.097 ± 0.006	−21.75	26	−0.87
7	305.2	0.925 ± 0.71	−16.44	20	−0.82
FLUC	261.3	2.02 ± 0.42	−14.60	18	−0.81
CMP	323.2	0.903 ± 0.107	−16.49	21	−0.79
AraCMP	243.1	18.91 ± 5.8	−9.34	21	−0.44
CDV	279.2	∼40	−7.57	18	−0.42

Table 6. Co-Crystallization Conditions for *Ec*IspF Complexes

no.	ligand conc (mM)	protein conc (mg mL^{-1})	salt	buffer (0.1 M)	precipitant	cryoprotectant
6/6b	2	5.5	0.2 M potassium sodium tartrate	trisodium citrate, pH 5.6	2.0 M ammonium sulfate	25% butanediol
7	2	10	2 M ammonium formate	HEPES, pH 7.5	5% butanediol	25% butanediol
CDV	2	5.5	0.5 M ammonium sulfate	trisodium citrate, pH 5.6	1 M lithium sulfate	25% MPD
FLUC	15	10	10% glycerol	magnesium sulfate	20% PEG 4000	
AraCMP	2	5.5	0.1 M ammonium sulfate	sodium acetate, pH 4.4	PEG 2000 MME	50% MPD

greater than 95% by SDS-PAGE and matrix-assisted laser desorption/ionization time-of-flight mass spectrometry.

SPR Biosensor Studies. SPR experiments were performed on a Biacore 3000 (Biacore, Uppsala, Sweden) instrument with CM5 research grade chips (Biacore, Uppsala, Sweden). Sensorgrams were recorded at a frequency of 2.5 Hz. *Ec*IspF was immobilized using amine-coupling chemistry. Briefly, the sensor chip surface was activated with three 6 min injections at 5 μL min^{-1} of a mixture of *N*-hydroxysuccinimide at 115 mg mL^{-1} and 1-ethyl-3-(3-dimethylaminopropyl) carbodiimide hydrochloride at 750 mg mL^{-1}. *Ec*IspF was diluted with 10 mM acetate buffer pH 5.5 to a final concentration of approximately 100 μg mL^{-1} and applied to the chip so that readings between 4500 and 5500 response units were obtained. After immobilization, a 6 min injection at 5 μL min^{-1} of 1 M ethanolamine was used to quench excess active succinamide ester groups. SPR binding experiments with *Ec*IspF were performed at 10 °C in 50 mM sodium phosphate pH 7 and 2 mM MgCl at a flow rate of 30 μL min^{-1}. The sensor surface was regenerated between experiments by applying the running buffer for 20 min to dissociate any ligand complex. This was followed by a further 20 min stabilization period. Immobilized *Ec*IspF is not amenable to more stringent and rapid regeneration conditions (data not shown). The 40 min total regeneration time between experiments helped to eliminate any carry-over of *Ec*IspF bound to ligand. A concentration series, ranging from 0.1 μM to 10 mM, of ligand was typically run in these experiments. Each injection at a given concentration was repeated three times. Blank injections were included for each measurement series and subtracted from the data. The equilibrium (steady state) binding curves were analyzed by nonlinear regression and fit to a one-to-one Langmuir binding model. All ligands assessed by SPR were greater than 95% purity as established by high-performance liquid chromatography or combustion analysis.

Crystallization and Structure Determination. Crystals were obtained by vapor diffusion at 20 °C with 3 μL hanging drops over a 250 μL reservoir solution. Ligand cocrystallization conditions varied depending on the ligand and protein concentrations (Table 6). After 1−10 days, crystals displaying one of two morphologies, cubic blocks or plates, grew to an average size of 0.4 mm and 0.4 × 0.4 × 0.05 mm^3, respectively. Crystals were harvested from the drops and soaked in a mixture of cryoprotectant (Table 6) and mother liquor for approximately 30 s and then cooled in a nitrogen gas stream at −170 °C for data collection. Data sets for *Ec*IspF in complex with **6b**, **7**, and AraCMP were measured on beamline ID29 with a Q210 2D detector (Area Detector Systems Corp.) at the European Synchrotron Radiation Facility, and *Ec*IspF in complex with CDV and FLUC were measured in-house using an RU-200 rotating-anode generator (Cu Kα, λ = 1.5418 Å) with an R-Axis IV image plate detector (Rigaku). Data were processed with MOSFLM[45] and scaled using the CCP4 program suite.[46] The complexes of *Ec*IspF with **7**, AraCMP, and FLUC were solved by molecular replacement with AMoRe[47] using a monomer from the published *Ec*IspF structure (PDB 1GX1). Complex structures of *Ec*Ispf with **6** and CDV were derived from the **7** complex structure by rigid body refinement. The models were refined with REFMAC[48] using established protocols,[49] together with several rounds of manual alteration in COOT[50] or O.[51] Superpositions were calculated using LSQMAN[52] and figures produced using PyMOL.[53]

Acknowledgment. Funded by the Scottish Funding Council, the Biotechnology and Biological Sciences Research Council BBS/B/14434, The Wellcome Trust 082596 and 083481, and Inpharmatica Ltd. We thank the European Synchrotron Radiation Facility, Grenoble, for synchrotron time, our colleagues for useful discussions, and Dr. John Butler for assistance with SPR.

References

(1) Beytia, E. D.; Porter, J. W. Biochemistry of polyisoprenoid biosynthesis. *Annu. Rev. Biochem.* **1976**, *45*, 113–142.
(2) Schwender, J.; Seemann, M.; Lichtenthaler, H. K.; Rohmer, M. Biosynthesis of isoprenoids (carotenoids, sterols, prenyl side chains of chlorophylls, and plastoquinone) via a novel pyruvate/glyceraldehyde 3-phosphate non-mevalonate pathway in the green alga *Scenedesmus obliquus*. *Biochem. J.* **1996**, *316* (Pt 1), 73–80.
(3) Rohdich, F.; Kis, K.; Bacher, A.; Eisenreich, W. The non-mevalonate pathway of isoprenoids: genes, enzymes, and intermediates. *Curr. Opin. Chem. Biol.* **2001**, *5*, 535–540.
(4) Hunter, W. N. The non-mevalonate pathway of isoprenoid precursor biosynthesis. *J. Biol. Chem.* **2007**, *282*, 21573–21577.
(5) Rohmer, M.; Knani, M.; Simonin, P.; Sutter, B.; Sahm, H. Isoprenoid biosynthesis in bacteria: a novel pathway for the early steps leading to isopentenyl diphosphate. *Biochem. J.* **1993**, *295*, 517–524.
(6) Rohmer, M. The discovery of a mevalonate-independent pathway for isoprenoid biosynthesis in bacteria, algae and higher plants. *Nat. Prod. Rep.* **1999**, *16*, 565–574.
(7) Cvejic, J. H.; Rohmer, M. CO_2 as main carbon source for isoprenoid biosynthesis via the mevalonate-independent methylerythritol 4-phosphate route in the marine diatoms *Phaeodactylum tricornutum* and *Nitzschia ovalis*. *Phytochemistry* **2000**, *53*, 21–28.
(8) Borza, T.; Popescu, C. E.; Lee, R. W. Multiple metabolic roles for the nonphotosynthetic plastid of the green alga *Prototheca wickerhamii*. *Eukaryotic Cell* **2005**, *4*, 253–261.
(9) Boucher, Y.; Doolittle, W. F. The role of lateral gene transfer in the evolution of isoprenoid biosynthesis pathways. *Mol. Microbiol.* **2000**, *37*, 703–716.
(10) Freiberg, C.; Wieland, B.; Spaltmann, F.; Ehlert, K.; Brotz, H.; Labischinski, H. Identification of novel essential *Escherichia coli* genes conserved among pathogenic bacteria. *J. Mol. Microbiol. Biotechnol.* **2001**, *3*, 483–489.
(11) Ridley, R. G. Planting the seeds of new antimalarial drugs. *Science* **1999**, *285*, 1502–1503.
(12) Campos, N.; Rodriguez-Concepcion, M.; Sauret-Gueto, S.; Gallego, F.; Lois, L. M.; Boronat, A. *Escherichia coli* engineered to synthesize isopentenyl diphosphate and dimethylallyl diphosphate from mevalonate: a novel system for the genetic analysis of the 2-*C*-methyl-D-erythritol 4-phosphate pathway for isoprenoid biosynthesis. *Biochem. J.* **2001**, *353*, 59–67.

(13) Missinou, M. A.; Borrmann, S.; Schindler, A.; Issifou, S.; Adegnika, A. A.; Matsiegui, P. B.; Binder, R.; Lell, B.; Wiesner, J.; Baranek, T.; Jomaa, H.; Kremsner, P. G. Fosmidomycin for malaria. *Lancet* **2002**, *360*, 1941–1942.
(14) Jomaa, H.; Wiesner, J.; Sanderbrand, S.; Altincicek, B.; Weidemeyer, C.; Hintz, M.; Turbachova, I.; Eberl, M.; Zeidler, J.; Lichtenthaler, H. K.; Soldati, D.; Beck, E. Inhibitors of the nonmevalonate pathway of isoprenoid biosynthesis as antimalarial drugs. *Science* **1999**, *285*, 1573–1576.
(15) Herz, S.; Wungsintaweekul, J.; Schuhr, C. A.; Hecht, S.; Luttgen, H.; Sagner, S.; Fellermeier, M.; Eisenreich, W.; Zenk, M. H.; Bacher, A.; Rohdich, F. Biosynthesis of terpenoids: YgbB protein converts 4-diphosphocytidyl-2*C*-methyl-D-erythritol 2-phosphate to 2*C*-methyl-D-erythritol 2,4-cyclodiphosphate. *Proc. Natl. Acad. Sci. U.S.A* **2000**, *97*, 2486–2490.
(16) Kemp, L. E.; Bond, C. S.; Hunter, W. N. Structure of 2*C*-methyl-D-erythritol 2,4- cyclodiphosphate synthase: an essential enzyme for isoprenoid biosynthesis and target for antimicrobial drug development. *Proc. Natl. Acad. Sci. U.S.A* **2002**, *99*, 6591–6596.
(17) Richard, S. B.; Ferrer, J. L.; Bowman, M. E.; Lillo, A. M.; Tetzlaff, C. N.; Cane, D. E.; Noel, J. P. Structure and mechanism of 2*C*-methyl-D-erythritol 2,4-cyclodiphosphate synthase. An enzyme in the mevalonate-independent isoprenoid biosynthetic pathway. *J. Biol. Chem.* **2002**, *277*, 8667–8672.
(18) Steinbacher, S.; Kaiser, J.; Wungsintaweekul, J.; Hecht, S.; Eisenreich, W.; Gerhardt, S.; Bacher, A.; Rohdich, F. Structure of 2*C*-methyl-D-erythritol-2,4-cyclodiphosphate synthase involved in mevalonate-independent biosynthesis of isoprenoids. *J. Mol. Biol.* **2002**, *316*, 79–88.
(19) Lehmann, C.; Lim, K.; Toedt, J.; Krajewski, W.; Howard, A.; Eisenstein, E.; Herzberg, O. Structure of 2*C*-methyl-D-erythrol-2,4-cyclodiphosphate synthase from *Haemophilus influenzae*: activation by conformational transition. *Proteins* **2002**, *49*, 135–138.
(20) Kishida, H.; Wada, T.; Unzai, S.; Kuzuyama, T.; Takagi, M.; Terada, T.; Shirouzu, M.; Yokoyama, S.; Tame, J. R.; Park, S. Y. Structure and catalytic mechanism of 2*C*-methyl-D-erythritol 2,4-cyclodiphosphate (MECDP) synthase, an enzyme in the non-mevalonate pathway of isoprenoid synthesis. *Acta Crystallogr., Sect. D: Biol. Crystallogr.* **2003**, *59*, 23–31.
(21) Buetow, L.; Brown, A. C.; Parish, T.; Hunter, W. N. The structure of *Mycobacteria* 2*C*-methyl-D-erythritol-2,4-cyclodiphosphate synthase, an essential enzyme, provides a platform for drug discovery. *BMC Struct. Biol.* **2007**, *7*, 68.
(22) Sgraja, T.; Kemp, L. E.; Ramsden, N.; Hunter, W. N. A double mutation of *Escherichia coli* 2*C*-methyl-D-erythritol-2,4-cyclodiphosphate synthase disrupts six hydrogen bonds with, yet fails to prevent binding of, an isoprenoid diphosphate. *Acta Crystallogr., Sect. F: Struct. Biol. Cryst. Commun.* **2005**, *61*, 625–629.
(23) Kemp, L. E.; Alphey, M. S.; Bond, C. S.; Ferguson, M. A.; Hecht, S.; Bacher, A.; Eisenreich, W.; Rohdich, F.; Hunter, W. N. The identification of isoprenoids that bind in the intersubunit cavity of *Escherichia coli* 2*C*-methyl-D-erythritol-2,4-cyclodiphosphate synthase by complementary biophysical methods. *Acta Crystallogr., Sect. D: Biol. Crystallogr.* **2005**, *61*, 45–52.
(24) Gabrielsen, M.; Bond, C. S.; Hallyburton, I.; Hecht, S.; Bacher, A.; Eisenreich, W.; Rohdich, F.; Hunter, W. N. Hexameric assembly of the bifunctional methylerythritol 2,4-cyclodiphosphate synthase and protein−protein associations in the deoxy-xylulose-dependent pathway of isoprenoid precursor biosynthesis. *J. Biol. Chem.* **2004**, *279*, 52753–52761.
(25) Gabrielsen, M.; Rohdich, F.; Eisenreich, W.; Gräwert, T.; Hecht, S.; Bacher, A.; Hunter, W. N. Biosynthesis of isoprenoids: a bifunctional IspDF enzyme from *Campylobacter jejuni*. *Eur. J. Biochem.* **2004**, *271*, 3028–3035.
(26) Rarey, M.; Kramer, B.; Lengauer, T.; Klebe, G. A fast flexible docking method using an incremental construction algorithm. *J. Mol. Biol.* **1996**, *261*, 470–489.
(27) Cole, J. C.; Murray, C. W.; Nissink, J. W.; Taylor, R. D.; Taylor, R. Comparing protein−ligand docking programs is difficult. *Proteins.* **2005**, *60*, 325–332.
(28) Gruneberg, S.; Wendt, B.; Klebe, G. Subnanomolar Inhibitors from Computer Screening: A Model Study Using Human Carbonic Anhydrase II. *Angew. Chem., Int. Ed.* **2001**, *40*, 389–393.
(29) Brenk, R.; Naerum, L.; Gradler, U.; Gerber, H. D.; Garcia, G. A.; Reuter, K.; Stubbs, M. T.; Klebe, G. Virtual screening for submicromolar leads of tRNA-guanine transglycosylase based on a new unexpected binding mode detected by crystal structure analysis. *J. Med. Chem.* **2003**, *46*, 1133–1143.
(30) Hann, M. M.; Leach, A. R.; Harper, G. Molecular complexity and its impact on the probability of finding leads for drug discovery. *J. Chem. Inf. Comput. Sci.* **2001**, *41*, 856–864.
(31) Oprea, T. I.; Davis, A. M.; Teague, S. J.; Leeson, P. D. Is there a difference between leads and drugs? A historical perspective. *J. Chem. Inf. Comput. Sci.* **2001**, *41*, 1308–1315.
(32) Crane, C. M.; Kaiser, J.; Ramsden, N. L.; Lauw, S.; Rohdich, F.; Eisenreich, W.; Hunter, W. N.; Bacher, A.; Diederich, F. Fluorescent inhibitors for IspF, an enzyme in the non-mevalonate pathway for isoprenoid biosynthesis and a potential target for antimalarial therapy. *Angew. Chem., Int. Ed.* **2006**, *45*, 1069–1074.
(33) Giebel, S.; Krawczyk-Kulis, M.; Adamczyk-Cioch, M.; Jakubas, B.; Palynyczko, G.; Lewandowski, K.; Dmoszynska, A.; Skotnicki, A.; Nowak, K.; Holowiecki, J. Fludarabine, cytarabine, and mitoxantrone (FLAM) for the treatment of relapsed and refractory adult acute lymphoblastic leukemia. A phase study by the Polish Adult Leukemia Group (PALG). *Ann. Hematol.* **2006**, *85*, 717–722.
(34) Holý, A. Antiviral acyclic nucleoside phosphonates structure activity studies. *Antiviral Res.* **2006**, *71*, 248–253.
(35) Rao, B. G. Recent developments in the design of specific matrix metalloproteinase inhibitors aided by structural and computational studies. *Curr. Pharm. Des.* **2005**, *11*, 295–322.
(36) Chen, M. H.; Steiner, M. G.; de Laszlo, S. E.; Patchett, A. A.; Anderson, M. S.; Hyland, S. A.; Onishi, H. R.; Silver, L. L.; Raetz, C. R. Carbohydroxamido-oxazolidines: antibacterial agents that target lipid A biosynthesis. *Bioorg. Med. Chem. Lett.* **1999**, *9*, 313–318.
(37) Teague, S. J.; Davis, A. M.; Leeson, P. D.; Oprea, T. The design of leadlike combinatorial Libraries. *Angew. Chem., Int. Ed.* **1999**, *38*, 3743–3748.
(38) Hopkins, A. L.; Groom, C. R.; Alex, A. Ligand efficiency: a useful metric for lead selection. *Drug Discovery Today* **2004**, *9*, 430–431.
(39) Hajduk, P. J. Fragment-based drug design: how big is too big? *J. Med. Chem.* **2006**, *49*, 6972–6976.
(40) Jackman, J. E.; Raetz, C. R.; Fierke, C. A. UDP-3-*O*-(*R*-3-hydroxymyristoyl)-*N*-acetylglucosamine deacetylase of *Escherichia coli* is a zinc metalloenzyme. *Biochemistry* **1999**, *38*, 1902–1911.
(41) *SELECTOR, Molecular Modelling Package*; Tripos Inc.: St. Louis, MO, 1996; 1699 South Hanley Road, St. Louis, MO 63144.
(42) *SYBYL, Molecular Modelling Package*; Tripos Inc.: St. Louis, MO, 1996; 1699 South Hanley Road, St. Louis, MO, 63144.
(43) Lipinski, C. Drug-like properties and the causes of poor solubility and poor permeability. *J. Pharmacol. Toxicol. Methods* **2000**, *44*, 235–249.
(44) Gohlke, H.; Hendlich, M.; Klebe, G. Knowledge-based scoring function to predict protein−ligand interactions. *J. Mol. Biol.* **2000**, *295*, 337–356.
(45) Leslie, A. G.; Powell, H. R.; Winter, G.; Svensson, O.; Spruce, D.; McSweeney, S.; Love, D.; Kinder, S.; Duke, E.; Nave, C. Automation of the collection and processing of X-ray diffraction data—a generic approach. *Acta Crystallogr., Sect. D: Biol. Crystallogr.* **2002**, *58*, 1924–1928.
(46) Collaborative Computational Project, Number 4. The CCP4 Suite: Programs for Protein Crystallography. *Acta Crystallogr., Sect. D: Biol. Crystallogr.* **1994**, *50*, 760−763.
(47) Navaza, J. Implementation of molecular replacement in AMoRe. *Acta Crystallogr., Sect. D: Biol. Crystallogr.* **2001**, *57*, 1367–1372.
(48) Murshudov, G. N.; Vagin, A. A.; Dodson, E. J. Refinement of macromolecular structures by the maximum-likelihood method. *Acta Crystallogr., Sect. D: Biol. Crystallogr.* **1997**, *53*, 240–255.
(49) Buetow, L.; Smith, T. K.; Dawson, A.; Fyffe, S.; Hunter, W. N. Structure and reactivity of LpxD, the *N*-acyltransferase of lipid A biosynthesis. *Proc. Natl. Acad. Sci. U.S.A.* **2007**, *104*, 4321–4326.
(50) Emsley, P.; Cowtan, K. Coot: model-building tools for molecular graphics. *Acta Crystallogr., Sect. D: Biol. Crystallogr.* **2004**, *60*, 2126–2132.
(51) Jones, T. A.; Zou, J. Y.; Cowan, S. W.; Kjeldgaard, M. Improved methods for building protein models in electron density maps and the location of errors in these models. *Acta Crystallogr., Sect. A: Found. Crystallogr.* **1991**, *47*, 110–119.
(52) Kleywegt, G. J. Use of non-crystallographic symmetry in protein structure refinement. *Acta Crystallogr., Sect. D: Biol. Crystallogr.* **1996**, *52*, 842–857.
(53) Warren, L. D. *The PyMOL Molecular Graphics System*; DeLano Scientific: San Carlos, CA, 2002.

JM801475N